

# Measurements of Production Properties of $K_S^0$ mesons and $\Lambda$ hyperons in Proton–Carbon Interactions at 31 GeV/c

N. Abgrall,<sup>1</sup> A. Aduszkiewicz,<sup>2</sup> Y. Ali,<sup>3</sup> T. Anticic,<sup>4</sup> N. Antoniou,<sup>5</sup> J. Argyriades,<sup>1</sup> B. Baatar,<sup>6</sup> A. Blondel,<sup>1</sup> J. Blumer,<sup>7</sup> M. Bogomilov,<sup>8</sup> A. Bravar,<sup>1</sup> W. Brooks,<sup>9</sup> J. Brzychczyk,<sup>3</sup> S. A. Bunyatov,<sup>6</sup> O. Busygina,<sup>10</sup> P. Christakoglou,<sup>5</sup> T. Czopowicz,<sup>11</sup> N. Davis,<sup>5</sup> S. Debieux,<sup>1</sup> H. Dembinski,<sup>7</sup> F. Diakonov,<sup>5</sup> S. Di Luise,<sup>12</sup> W. Dominik,<sup>2</sup> T. Drozhzhova,<sup>13</sup> J. Dumarchez,<sup>14</sup> K. Dynowski,<sup>11</sup> R. Engel,<sup>7</sup> A. Ereditato,<sup>15</sup> L. Esposito,<sup>12</sup> G. A. Feofilov,<sup>13</sup> Z. Fodor,<sup>16</sup> A. Fulop,<sup>16</sup> M. Gaździcki,<sup>17,18</sup> M. Golubeva,<sup>10</sup> K. Grebieszko,<sup>11</sup> A. Grzeszczuk,<sup>19</sup> F. Guber,<sup>10</sup> H. Hakobyan,<sup>9</sup> A. Haesler,<sup>1</sup> T. Hasegawa,<sup>20</sup> M. Hierholzer,<sup>15</sup> R. Idczak,<sup>21</sup> S. Igotkin,<sup>13</sup> Y. Ivanov,<sup>9</sup> A. Ivashkin,<sup>10</sup> D. Jokovic,<sup>22</sup> K. Kadija,<sup>4</sup> A. Kapoyannis,<sup>5</sup> N. Katrynska,<sup>21</sup> E. Kaptur,<sup>19</sup> D. Kielcewska,<sup>2</sup> D. Kikola,<sup>11</sup> M. Kirejczyk,<sup>2</sup> J. Kisiel,<sup>19</sup> T. Kiss,<sup>16</sup> S. Kleinfelder,<sup>23</sup> T. Kobayashi,<sup>20</sup> V. I. Kolesnikov,<sup>6</sup> D. Kolev,<sup>8</sup> V. P. Kondratiev,<sup>13</sup> A. Korzenev,<sup>1</sup> S. Kowalski,<sup>19</sup> A. Krasnoperov,<sup>6</sup> S. Kuleshov,<sup>9</sup> A. Kurepin,<sup>10</sup> D. Larsen,<sup>24</sup> A. Laszlo,<sup>16</sup> V. V. Lyubushkin,<sup>6</sup> M. Mackowiak-Pawłowska,<sup>18,11</sup> Z. Majka,<sup>3</sup> B. Maksiak,<sup>11</sup> A. I. Malakhov,<sup>6</sup> D. Maletic,<sup>22</sup> D. Manic,<sup>22</sup> A. Marchionni,<sup>12</sup> A. Marcinek,<sup>3</sup> V. Marin,<sup>10</sup> K. Marton,<sup>16</sup> H.-J. Mathes,<sup>7</sup> T. Matulewicz,<sup>2</sup> V. Matveev,<sup>10,6</sup> G. L. Melkumov,<sup>6</sup> St. Mrówczyński,<sup>17</sup> S. Murphy,<sup>1</sup> T. Nakadaira,<sup>20</sup> M. NirKKo,<sup>15</sup> K. Nishikawa,<sup>20</sup> T. Palczewski,<sup>25</sup> G. Palla,<sup>16</sup> A. D. Panagiotou,<sup>5</sup> T. Paul,<sup>26</sup> W. Peryt,<sup>11</sup> C. Pistillo,<sup>15</sup> A. Redij,<sup>15</sup> O. Petukhov,<sup>10</sup> R. Planeta,<sup>3</sup> J. Pluta,<sup>11</sup> B. A. Popov,<sup>6,14</sup> M. Posiadała,<sup>2</sup> S. Puławski,<sup>19</sup> J. Puzovic,<sup>22</sup> W. Rauch,<sup>27</sup> M. Ravonel,<sup>1</sup> R. Renfordt,<sup>18</sup> A. Robert,<sup>14</sup> D. Röhrich,<sup>24</sup> E. Rondio,<sup>25</sup> M. Roth,<sup>7</sup> A. Rubbia,<sup>12</sup> A. Rustamov,<sup>18</sup> M. Rybczynski,<sup>17</sup> A. Sadovsky,<sup>10</sup> K. Sakashita,<sup>20</sup> M. Savic,<sup>22</sup> K. Schmidt,<sup>19</sup> T. Sekiguchi,<sup>20</sup> P. Seyboth,<sup>17</sup> M. Shibata,<sup>20</sup> R. Sipos,<sup>16</sup> E. Skrzypczak,<sup>2</sup> M. Slodkowski,<sup>11</sup> P. Staszczel,<sup>3</sup> G. Stefanek,<sup>17</sup> J. Stepaniak,<sup>25</sup> T. Susa,<sup>4</sup> M. Szuba,<sup>7</sup> M. Tada,<sup>20</sup> V. Tereshchenko,<sup>6</sup> T. Tolyhi,<sup>16</sup> R. Tsenov,<sup>8</sup> L. Turko,<sup>21</sup> R. Ulrich,<sup>7</sup> M. Unger,<sup>7</sup> M. Vassiliou,<sup>5</sup> D. Veberic,<sup>26</sup> V. V. Vechernin,<sup>13</sup> G. Vesztegombi,<sup>16</sup> L. Vinogradov,<sup>13</sup> A. Wilczek,<sup>19</sup> Z. Włodarczyk,<sup>17</sup> A. Wojtaszek,<sup>17</sup> O. Wyszynski,<sup>3</sup> L. Zambelli,<sup>14</sup> and W. Zipper<sup>19</sup>

## (The NA61/SHINE Collaboration)

<sup>1</sup>University of Geneva, Geneva, Switzerland

<sup>2</sup>Faculty of Physics, University of Warsaw, Warsaw, Poland

<sup>3</sup>Jagiellonian University, Cracow, Poland

<sup>4</sup>Rudjer Boskovic Institute, Zagreb, Croatia

<sup>5</sup>University of Athens, Athens, Greece

<sup>6</sup>Joint Institute for Nuclear Research, Dubna, Russia

<sup>7</sup>Karlsruhe Institute of Technology, Karlsruhe, Germany

<sup>8</sup>Faculty of Physics, University of Sofia, Sofia, Bulgaria

<sup>9</sup>The Universidad Tecnica Federico Santa Maria, Valparaiso, Chile

<sup>10</sup>Institute for Nuclear Research, Moscow, Russia

<sup>11</sup>Warsaw University of Technology, Warsaw, Poland

<sup>12</sup>ETH, Zurich, Switzerland

<sup>13</sup>St. Petersburg State University, St. Petersburg, Russia

<sup>14</sup>LPNHE, University of Paris VI and VII, Paris, France

<sup>15</sup>University of Bern, Bern, Switzerland

<sup>16</sup>Wigner Research Centre for Physics of the Hungarian Academy of Sciences, Budapest, Hungary

<sup>17</sup>Jan Kochanowski University in Kielce, Poland

<sup>18</sup>University of Frankfurt, Frankfurt, Germany

<sup>19</sup>University of Silesia, Katowice, Poland

<sup>20</sup>Institute for Particle and Nuclear Studies, KEK, Tsukuba, Japan

<sup>21</sup>University of Wrocław, Wrocław, Poland

<sup>22</sup>University of Belgrade, Belgrade, Serbia

<sup>23</sup>University of California, Irvine, USA

<sup>24</sup>University of Bergen, Bergen, Norway

<sup>25</sup>National Center for Nuclear Research, Warsaw, Poland

<sup>26</sup>Laboratory of Astroparticle Physics, University Nova Gorica, Nova Gorica, Slovenia

<sup>27</sup>Fachhochschule Frankfurt, Frankfurt, Germany

(Dated: September 10, 2013)

Spectra of  $K_S^0$  mesons and  $\Lambda$  hyperons were measured in p+C interactions at 31 GeV/c with the large acceptance NA61/SHINE spectrometer at the CERN SPS. The data were collected with an isotropic graphite target with a thickness of 4% of a nuclear interaction length. Interaction cross sections, charged pion spectra, and charged kaon spectra were previously measured using the same data set. Results on  $K_S^0$  and  $\Lambda$  production in p+C interactions serve as reference for the understanding of the enhancement of strangeness production in nucleus-nucleus collisions. Moreover,

they provide important input for the improvement of neutrino flux predictions for the T2K long baseline neutrino oscillation experiment in Japan.

Inclusive production cross sections for  $K_S^0$  and  $\Lambda$  are presented as a function of laboratory momentum in intervals of the laboratory polar angle covering the range from 0 up to 240 mrad. The results are compared with predictions of several hadron production models. The  $K_S^0$  mean multiplicity in production processes  $\langle n_{K_S^0} \rangle$  and the inclusive cross section for  $K_S^0$  production  $\sigma_{K_S^0}$  were measured and amount to  $0.127 \pm 0.005$  (stat)  $\pm 0.022$  (sys) and  $29.0 \pm 1.6$  (stat)  $\pm 5.0$  (sys) mb, respectively.

PACS numbers: 13.85.Lg,13.85.Hd,13.85.Ni

Keywords: p+C interaction, strangeness production, inclusive  $K_S^0$  and  $\Lambda$  spectra

## I. INTRODUCTION

Experimental data on strange particle production in proton-proton and proton-carbon interactions in the region below few tens of GeV/c incident momentum are scarce [1–4]. There are at least two reasons why the knowledge of yields of strange mesons and baryons are of considerable interest at the beam momentum of 31 GeV/c. One is the need to include the tuned production of these particles in the precise neutrino flux calculation for accelerator neutrino experiments as an additional source of neutrinos and secondary pions. Production of neutral kaons is important for accurate calculation of the  $\nu_e$  and  $\bar{\nu}_e$  flux from  $K_L^0 \rightarrow \pi e \nu_e$  decays. The other is the understanding of the production of strangeness in nucleus-nucleus interactions in this energy region and its proposed interpretation as a signal of the onset of deconfinement. Hadron-nucleus interactions constitute an intermediate step between proton-proton and nucleus-nucleus interactions. Therefore their study permits to understand better the influence of nuclear matter on strangeness production and can help to understand the role of the nucleus and non-exotic mechanisms of strangeness production. In addition to the primary goal of providing reference data for the T2K neutrino experiment in Japan, precise results on particle production in p+C interactions furnish important input to improve hadronic event generators which are required for the interpretation of air showers initiated by ultra high energy cosmic particles. The NA61/SHINE collaboration already published results on charged pion [5] and  $K^+$  production [6]. In this paper we present results on  $K_S^0$  and  $\Lambda$  yields. These were obtained from the analysis of the same sample of p+C collisions at 31 GeV/c beam momentum collected with the NA61/SHINE large acceptance spectrometer at the CERN SPS in 2007. The statistics of this data sample is insufficient to obtain results on  $\bar{\Lambda}$  yields, which are about 100 times smaller than  $\Lambda$  yields [7].

The paper is organized as follows. Section II provides information about the NA61/SHINE experimental apparatus. The main components of the detector and trigger system are presented. In addition, the target used is described and numbers of registered proton interactions are provided. The analysis technique is discussed in Section III. In this Section, the procedure of the extraction of the  $K_S^0$  mesons and  $\Lambda$  hyperons is described in detail.

The calculation of corrections and the normalization procedure are discussed. Subsection III A presents event and track selection criteria as well as the adopted phase space binning scheme. Information about extraction of the  $K_S^0$  mesons and  $\Lambda$  hyperons from the data and calculation of the correction factors used to correct raw yields for detector and other effects are described in Subsections III B and III C, respectively. The main sources of the systematic uncertainty are discussed in Subsection III D. The final results are shown in Section IV. They are compared to predictions of different hadron production models in Section V. Finally, Section VI summarizes the results of the paper.

## II. THE NA61/SHINE EXPERIMENTAL SET-UP

The NA61/SHINE experiment [8] is situated in the North Area H2 beam-line of the CERN SPS. It is the successor of the NA49 experiment [9]. The NA61/SHINE detector is a large acceptance hadron spectrometer, which consists of a set of large volume Time Projection Chambers (TPCs) and Time-of-Flight (ToF) scintillator walls. The schematic layout of the detector is shown in Fig. 1 together with the overall dimensions. Two of the TPCs (VTPC-1 and VTPC-2) are placed in the magnetic field produced by two super-conducting dipole magnets with maximum combined bending power of 9 Tm. During the 2007 data taking period the magnetic field was set to a bending power of 1.14 Tm to optimize the detector acceptance for the measurements needed for the T2K experiment. The TPCs were filled with Ar:CO<sub>2</sub> gas mixtures in proportions 90:10 for the VTPCs and 95:5 for the MTPCs. A set of scintillation and Cherenkov counters as well as beam position detectors (BPDs) upstream of the main detection system provided timing reference, identification and position measurements of the incoming beam particles. The 31 GeV/c secondary hadron beam was produced from 400 GeV protons extracted from the SPS in slow extraction mode. The secondary beam was transported along the H2 beam-line towards the experiment. Collimators in the beam line were adjusted to get an average beam particle rate of 15 kHz. Protons in the beam were identified by two Cherenkov counters, a CEDAR and a threshold counter, labeled C1 and C2, respectively. Two scintillation counters, S1 and S2, together with two

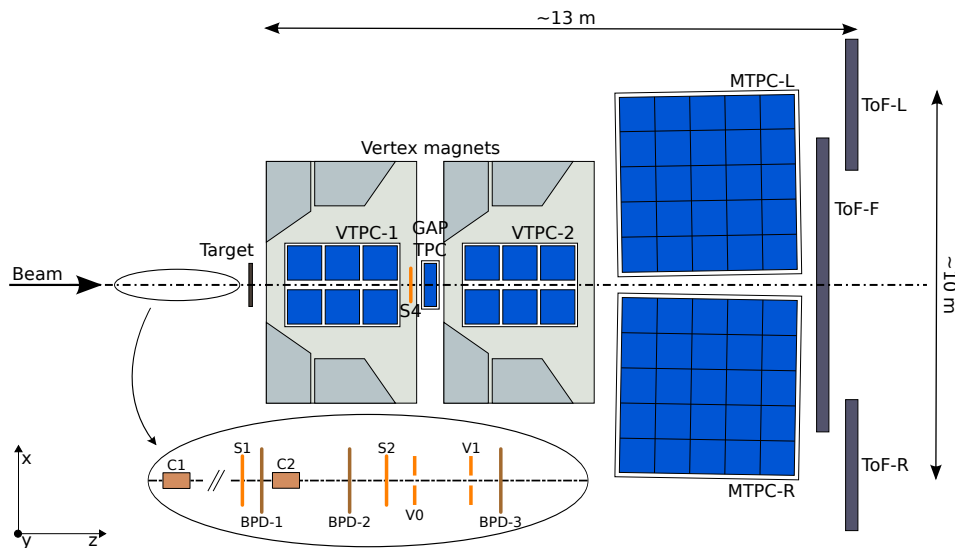


Figure 1: The NA61/SHINE experimental apparatus, see text for details.

veto counters, V0 and V1, were used to select beam particles. The S1 counter also provided the timing (start time for all counters). Beam protons were selected by the coincidence  $S1 \cdot S2 \cdot \overline{V0} \cdot \overline{V1} \cdot C1 \cdot \overline{C2}$ . The trajectory of individual beam particles is measured in the BPDs along the beam line. These counters are small ( $3 \times 3 \text{ cm}^2$ ) proportional chambers with cathode strip readout (BPD-1/2/3 in Fig. 1). A special run was taken to measure the beam momentum by bending the incoming beam particles into the TPCs with the full magnetic field. From this measurement the mean momentum value of  $30.75 \text{ GeV}/c$  was obtained. Interactions in the target were selected by an anti-coincidence of the incoming beam protons with a small, 2 cm diameter, scintillation counter (S4) placed on the beam trajectory between the two vertex magnets (see Fig. 1). This minimum bias trigger was based on the disappearance of the incident proton. The results presented here were obtained from  $667 \times 10^3$  proton interactions recorded with an isotropic graphite target of dimensions  $2.5(\text{W}) \times 2.5(\text{H}) \times 2(\text{L}) \text{ cm}^3$  and with a density of  $\rho = 1.84 \text{ g/cm}^3$ . For normalization purposes  $46 \times 10^3$  proton interactions with the carbon target removed were also recorded. The carbon target was installed 80 cm in front of VTPC-1.

### III. ANALYSIS TECHNIQUE

The most frequent decays of  $K_S^0$  mesons and  $\Lambda$  hyperons lead to the production of two oppositely charged particles. The measurement of particle tracks in the magnetic field allows to determine their charges and momenta. This section presents the method of  $K_S^0$  and  $\Lambda$  analysis using invariant mass distributions. When the  $K_S^0$  hypothesis is studied, positively (negatively) charged tracks are assumed to be  $\pi^+$  ( $\pi^-$ ) mesons. For the  $\Lambda$  hy-

pothesis the positively (negatively) charged particles are assumed to be protons ( $\pi^-$  mesons). The analysis was made in specific invariant mass windows. The selected window should cover the invariant mass peak of  $K_S^0$  ( $\Lambda$ ) but also include regions below and above the peak for the background estimate. Fits of the background function depend somewhat on the selected side regions. This effect was checked and added to the systematic uncertainties (see Sec. III D). The number of  $K_S^0$  and  $\Lambda$  was determined from fitting a sum of Lorentzian function and polynomial function for the signal and the background, respectively. The Lorentzian function is described by

$$f(x) = A \frac{\frac{1}{2}F}{(x - x_0)^2 + (\frac{1}{2}F)^2}, \quad (1)$$

where parameter  $A$  controls the height of the peak,  $F$  is the full width at half maximum (FWHM), and  $x_0$  is the mean value (in this case, the fitted  $K_S^0$  or  $\Lambda$  mass). The low statistics data forced to constrain the width of the signal function according to the Monte Carlo predictions. Namely, the width from Monte Carlo was set as initial value. Then, this parameter was allowed to vary (for  $K_S^0$  up to  $\pm 5 \cdot \Delta F_{\text{MC}}$ , where  $\Delta F_{\text{MC}}$  is an error of the fitted Monte Carlo width in a given  $\{p, \theta\}$  bin; for  $\Lambda$  up to  $\pm 7 \cdot \Delta F_{\text{MC}}$ ). The influence of this assumption on the final result was checked and added to the systematic uncertainties (see Sec. III D). In the standard approach a  $4^{\text{th}}$  order polynomial was used as the background function. The sensitivity to different shapes of the background function was studied and is included in the systematic uncertainties (see Sec. III D). The raw number of  $K_S^0$  and  $\Lambda$  was calculated as the integral of the fitted signal function Eq. 1. Corrections were applied to the raw numbers of  $K_S^0$  and  $\Lambda$  in order to obtain their yields produced in the primary p+C interac-

tions after strong and electromagnetic decays. Correction factors were derived from a Monte Carlo procedure in which events were generated from the hadron production model VENUS 4.12 [10] and then sent through a full simulation of the detector. The procedure takes into account the trigger bias, the vertex fit requirement and cuts, the branching ratio for the studied type of decay, the geometrical acceptance, the reconstruction efficiency and feed-down from interactions with the target material. The feed-down correction also takes into account  $\Lambda$  hyperons coming from secondary vertices. The inverse multiplicative Monte Carlo correction is calculated using the following formula

$$E(p, \theta) = \left( \frac{n_x}{N} \right)_{\text{acc}}^{\text{MC}} / \left( \frac{n_x}{N} \right)_{\text{gen}}^{\text{MC}} \quad (2)$$

which compares the information on simulated particles at the primary hadron generator level (gen) with that on reconstructed identified particles (acc). The quantity  $n_x$  is the number of the identified particle of type  $x$  ( $K_S^0$  or  $\Lambda$ ) in a given bin of phase-space,  $N$  is the number of events. The correction can be split into two parts: the first one connected with correction of numbers of a given particle of type  $x$  in a given bin ( $n_x^{\text{acc}}/n_x^{\text{gen}}$  which will be denoted  $\gamma$ ) and the second one connected with the correction of number of events ( $N^{\text{acc}}/N^{\text{gen}}$  which will be denoted  $\eta$ ). Therefore, the correction can be rewritten as follows:

$$E(p, \theta) = \left( \frac{n_x^{\text{acc}}}{n_x^{\text{gen}}} \right)^{\text{MC}} / \left( \frac{N^{\text{acc}}}{N^{\text{gen}}} \right)^{\text{MC}} = \frac{\gamma}{\eta} . \quad (3)$$

The subtraction of non-target interactions was performed using information from events recorded with target removed. The normalization was obtained far away from the target where all reconstructed vertices originate from interactions with the detector material (neglecting the beam attenuation in the target). The number of particles per event in a given phase space bin, corrected for non-target interactions, is calculated as:

$$\frac{n}{N} = \frac{1}{E} \frac{N^{\text{I}} - Bn^{\text{R}}}{N^{\text{I}} - BN^{\text{R}}} , \quad (4)$$

where I and R superscripts indicate data with target inserted and removed, respectively. The factor B is calculated from the data:

$$B = \frac{N_{\text{beam}}^{\text{I}}}{N_{\text{beam}}^{\text{R}}} = \frac{N_{\text{far } z}^{\text{I}}}{N_{\text{far } z}^{\text{R}}} , \quad (5)$$

where  $N_{\text{beam}}^{\text{R/I}}$  is the number of beam particles in data with target removed and inserted, respectively, and  $N_{\text{far } z}^{\text{R/I}}$  is the corresponding number of events with fitted vertex longitudinal coordinate,  $z$ , far away from the target. The differential spectrum is calculated as

$$\frac{dn}{dp} = \frac{n}{N} \frac{1}{\Delta p} . \quad (6)$$

Then the differential cross section is calculated as:

$$\frac{d\sigma}{dp} = \sigma_{\text{prod}} \frac{dn}{dp} , \quad (7)$$

where  $\sigma_{\text{prod}}$  is equal to  $229.3 \pm 1.9 \pm 9.0$  mb. The uncertainties on  $\sigma_{\text{prod}}$  were not included in the uncertainties of the final results presented in this paper. The measurements of the inelastic and production cross sections are presented in Ref. [11].

### A. Event and track selection, data binning

The analysis is based on  $667 \times 10^3$  event triggers with the graphite target inserted and  $46 \times 10^3$  triggers with the target removed. Only events with a properly reconstructed beam track were retained. First of all, the information from the Beam Position Detectors, placed upstream of the target (see Fig. 1), was used to ensure a well-defined beam track (see Ref. [8] for details). Then, events with reconstructed primary vertex, within the target (vertex  $z$  position within the range  $[-585.0, -575.0]$  cm), were selected in order to reject interactions that did not take place in the target but in the surrounding detector material. Any pair of tracks with opposite charges and distance of closest approach smaller than 1 cm was taken as a possible  $V^0$  candidate. In order to purify the sample and select candidates which correspond to  $K_S^0$  or  $\Lambda$  with high probability additional cuts were applied:

- (i) The distance along the beam direction between the primary vertex and the  $V^0$  decay point had to be larger than 3 cm. This cut was used to reject cases in which primary vertex tracks were wrongly reconstructed as  $V^0$  tracks. The same minimum distance cut was used for  $K_S^0$  and  $\Lambda$ . Although the decay lengths of the two particles are different, the signal to background ratio are very similar using the same cut.
- (ii) The  $V^0$  momentum vector had to point back to the primary vertex within a cut of  $d_x$  and  $d_y < 3$  cm in the transverse  $\{x, y\}$  plane for  $K_S^0$  and  $\Lambda$  candidates.
- (iii) The analysis was performed in the invariant mass windows  $[0.35, 0.7]$  GeV/ $c^2$  and  $[1.09, 1.16]$  GeV/ $c^2$  for  $K_S^0$  and  $\Lambda$ , respectively.
- (iv) A cut was applied on the angle between the momentum of the  $V^0$  candidate and its decay products in the c.m. system. Due to the expected isotropy of the decay in the  $V^0$  rest frame the distribution of the cosine of this angle ( $\cos \epsilon$ ) should be flat. The cut was set to  $-0.95 < \cos \epsilon < 0.8$  and  $-0.8 < \cos \epsilon < 0.8$  for  $K_S^0$  and  $\Lambda$ , respectively.
- (v) Cuts in the Armenteros-Podolanski plot were applied. The relation between Armenteros transverse momentum ( $p_{\text{T}}^{\text{arm}}$ ) and longitudinal momentum asymmetry ( $\alpha$ ) can be used to separate  $K_S^0$

mesons from  $\Lambda$  hyperons with high probability. The separation of  $K_S^0$  and  $\Lambda$  candidates using the Armenteros-Podolanski plot is shown in Fig. 2. For the selection of  $K_S^0$  candidates, the regions  $p_T^{\text{arm}} < 0.05$  and  $\alpha > 0.5$  and  $p_T^{\text{arm}} < 0.12$  is rejected in order to get rid of background originating from  $\Lambda$  particles. For the  $\Lambda$  selection, the region  $p_T^{\text{arm}} < 0.03$  or  $> 0.11$  was excluded. Furthermore, the region  $\alpha < 0.45$  was rejected.

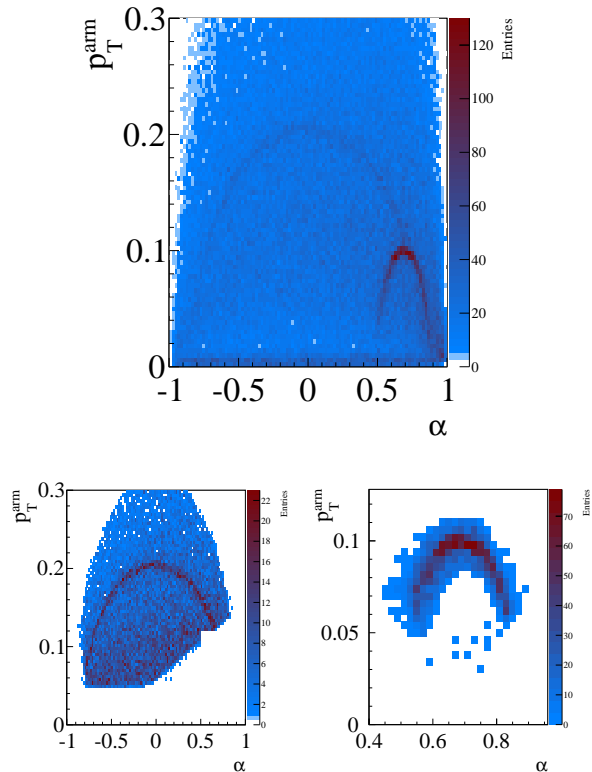


Figure 2: Armenteros-Podolanski plots before (top) and after all cuts for  $K_S^0$  (bottom left) and  $\Lambda$  candidates (bottom right).

The  $K_S^0$  candidate momentum vs polar angle distribution after event, track and  $V^0$  selection cuts is shown in Fig. 3 with superimposed binning. The bins colored in red were more sensitive to the model dependent corrections because for them the uncertainty of the shape of the event generator distributions could significantly affect the final results.

### B. Raw Yields

The  $(\pi^+\pi^-)$  invariant mass distributions in selected  $\{p, \theta\}$  bins for  $K_S^0$  candidates are presented in Fig. 4. The invariant mass distributions for  $\Lambda$  candidates in selected  $\{p, \theta\}$  bins are presented in Fig. 5. The raw number of

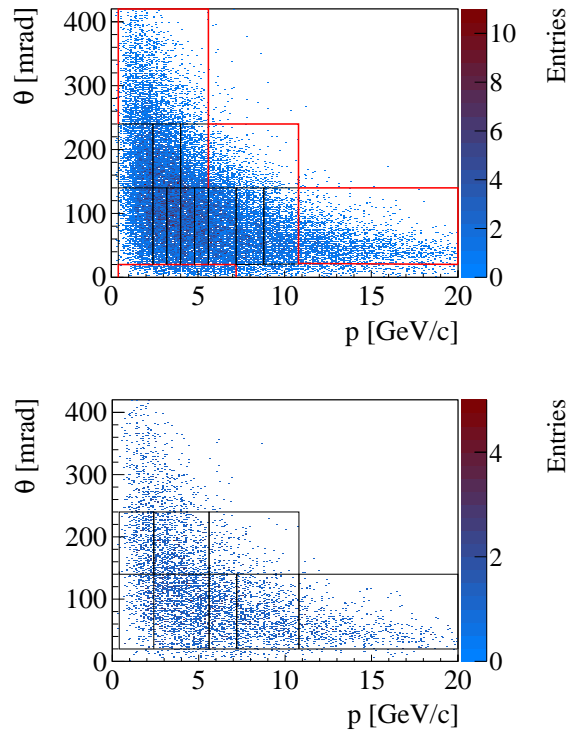


Figure 3: The momentum vs polar angle distributions for  $K_S^0$  (top) and  $\Lambda$  (bottom) candidates with superimposed binning.

$K_S^0$  and  $\Lambda$  extracted in the selected momentum and polar angle intervals is presented in Table I.

Table I: The raw number of  $K_S^0$  and  $\Lambda$  extracted by the fitting procedure in selected momentum and polar angle intervals

$\theta_{\text{low}}$ $\theta_{\text{up}}$ (mrad)		$K_S^0$				$\Lambda$			
		$p_{\text{low}}$ (GeV/c)	$p_{\text{up}}$ (GeV/c)	n	$\Delta n$	$p_{\text{low}}$ (GeV/c)	$p_{\text{up}}$ (GeV/c)	n	$\Delta n$
0	20	0.4	7.2	61	10				
20	140	0.4	2.4	178	23	0.4	2.4	53	8
		2.4	3.2	167	18	2.4	5.6	562	26
		3.2	4.0	165	18				
		4.0	4.8	126	18				
		4.8	5.6	132	16				
		5.6	7.2	130	16	5.6	7.2	248	16
		7.2	8.8	80	15	7.2	10.8	468	22
		8.8	10.8	115	15				
		10.8	20.0	102	17	10.8	20.0	362	19
140	240	0.4	2.4	93	15	0.4	2.4	60	12
		2.4	4.0	233	20	2.4	5.6	344	20
		4.0	5.6	135	20				
		5.6	10.8	88	12	5.6	10.8	72	17
240	420	0.4	5.6	135	26				

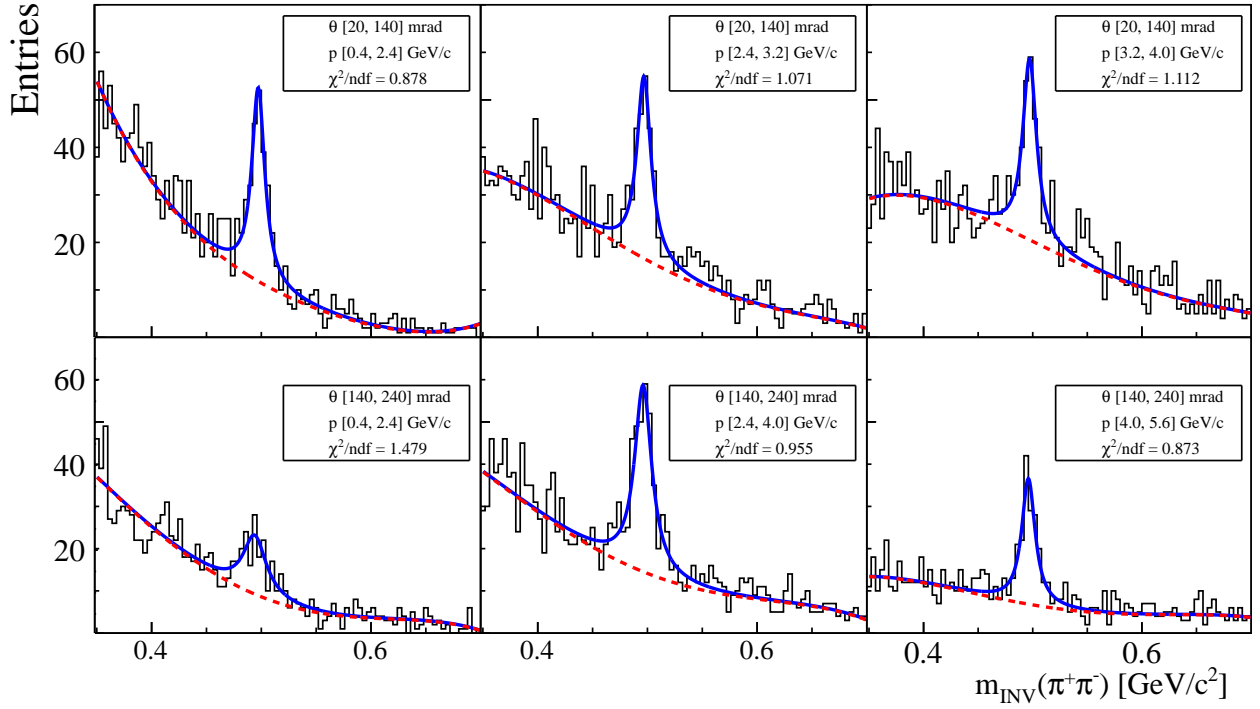


Figure 4: The invariant mass distributions for  $K_S^0$  candidates in selected  $\{p, \theta\}$  bins. Data (black) with superimposed background function (red dashed) and global fit (blue solid) are shown.

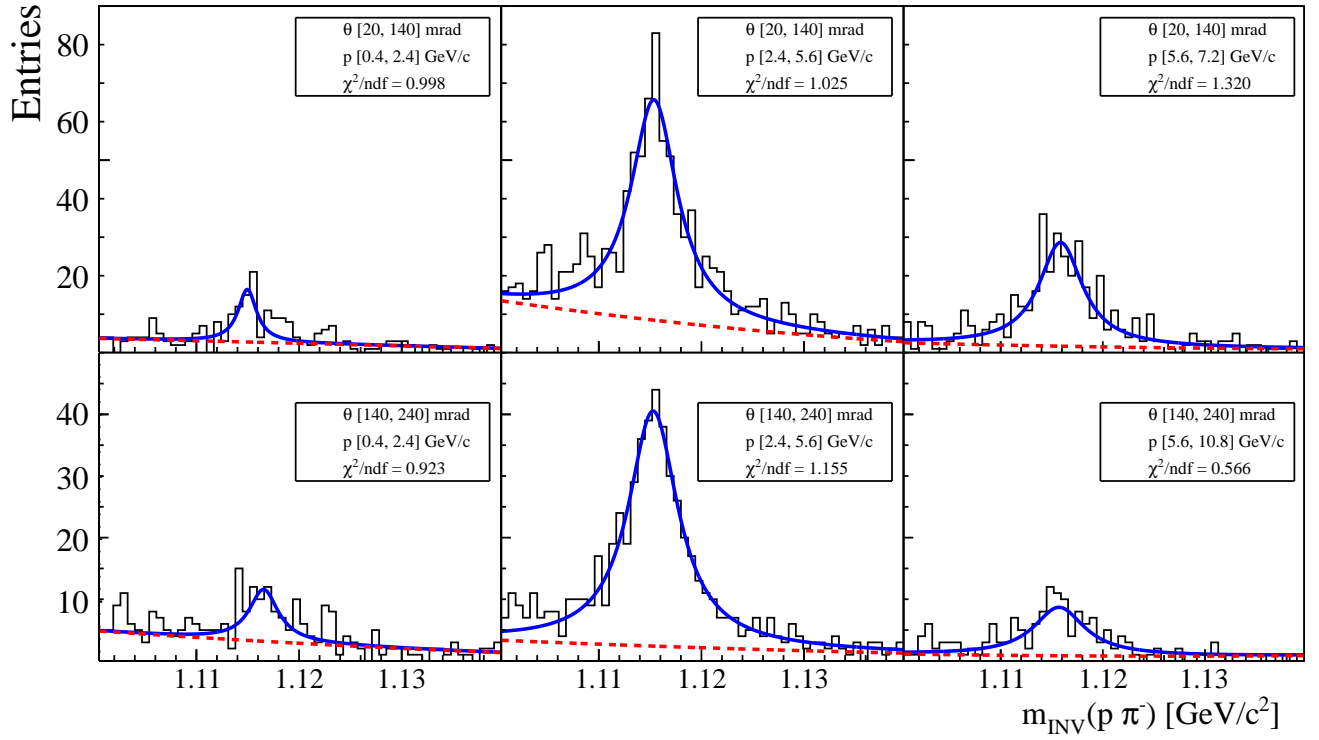


Figure 5: The invariant mass distributions for  $\Lambda$  candidates in selected  $\{p, \theta\}$  bins. Data (black) with superimposed background function (red dashed) and global fit (blue solid) are shown.

### C. Corrections

The simulation chain described in Ref. [5] was used to correct raw yields for detector effects (i.e. geometrical acceptance, reconstruction efficiency, resolution of  $p$  and  $\theta$  measurements), contributions from non-primary  $V^0$  decays, and decay branching ratios. The correction factor was calculated according to Eq. 2. For this calculation information from the simulation about reconstructed and simulated particles of each type is needed. The number of reconstructed particles is obtained in the same way as for the real data as the result of the integration of the fitted signal function after background subtraction. The momentum versus polar angle distribution of simulated  $K_S^0$  and  $\Lambda$  from the employed VENUS 4.12 model [10] is presented in Fig. 6.

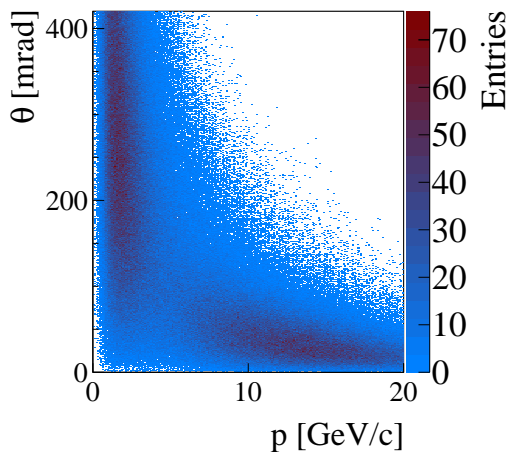
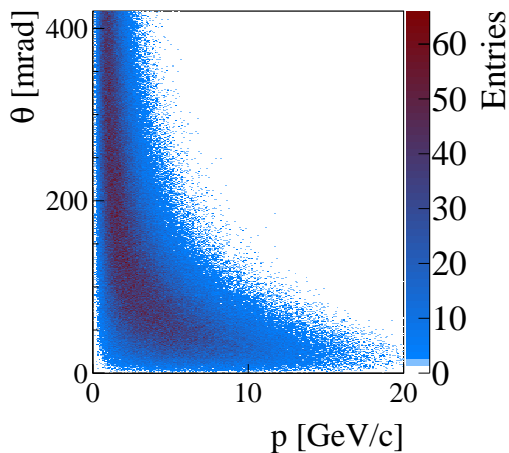


Figure 6: The momentum versus polar angle distribution for simulated  $K_S^0$  mesons (top) and  $\Lambda$  hyperons (bottom).

The invariant mass distributions for  $K_S^0$  and  $\Lambda$  candidates in selected  $\{p, \theta\}$  bins are presented in Figs. 7 and 8, respectively.

The correction factors  $\gamma$  for  $K_S^0$  and  $\Lambda$  (see Eq. 3) were evaluated in bins of momentum and polar angle variables and are presented in Table II and Table III, respectively. The correction factor  $\eta$  is bin independent and was estimated to be equal to  $0.8083 \pm 0.0005$ .

Table II: The number of simulated  $K_S^0$  ( $n_{\text{sim}}$ ), number of  $K_S^0$  found by the fitting procedure ( $n_{\text{rec}}$ ), the  $\gamma$ -correction factor, and their errors in selected momentum and polar angle intervals.

$\theta_{\text{low}}$ (mrad)	$\theta_{\text{up}}$ (mrad)	$p_{\text{low}}$ (GeV/c)	$p_{\text{up}}$ (GeV/c)	$n_{\text{sim}}$	$\Delta n_{\text{sim}}$	$n_{\text{rec}}$	$\Delta n_{\text{rec}}$	$\gamma$	$\Delta \gamma$
0	20	0.4	7.2	10908	104	1067	37	0.0979	0.0035
20	140	0.4	2.4	58087	241	2417	55	0.0416	0.001
		2.4	3.2	32905	181	2472	59	0.0751	0.0018
		3.2	4.0	31544	178	2624	62	0.0831	0.0020
		4.0	4.8	28274	168	2574	62	0.0910	0.0022
		4.8	5.6	24330	156	2241	57	0.0921	0.0024
		5.6	7.2	36936	192	3345	71	0.0905	0.0020
		7.2	8.8	24172	155	2325	60	0.0962	0.0025
		8.8	10.8	18054	134	1726	52	0.0956	0.0029
		10.8	20.0	16742	129	1521	54	0.0909	0.0033
140	240	0.4	2.4	69280	263	1359	45	0.0196	0.0006
		2.4	4.0	31443	177	2548	61	0.0810	0.0020
		4.0	5.6	10373	102	1417	46	0.1366	0.0046
		5.6	10.8	4250	65	661	34	0.1557	0.0083
240	420	0.4	5.6	119075	345	2209	61	0.0185	0.0005

Table III: The number of simulated  $\Lambda$  ( $n_{\text{sim}}$ ), number of  $\Lambda$  found by the fitting procedure ( $n_{\text{rec}}$ ),  $\gamma$  correction factor, and their errors in selected momentum and polar angle intervals.

$\theta_{\text{low}}$ (mrad)	$\theta_{\text{up}}$ (mrad)	$p_{\text{low}}$ (GeV/c)	$p_{\text{up}}$ (GeV/c)	$n_{\text{sim}}$	$\Delta n_{\text{sim}}$	$n_{\text{rec}}$	$\Delta n_{\text{rec}}$	$\gamma$	$\Delta \gamma$
20	140	0.4	2.4	38316	196	1557	43	0.041	0.001
		2.4	5.6	62777	250	7081	90	0.113	0.001
		5.6	7.2	30357	174	3896	64	0.128	0.002
		7.2	10.8	79015	281	9122	95	0.115	0.001
		10.8	20.0	121755	349	10883	102	0.089	0.001
140	240	0.4	2.4	61866	249	2377	52	0.038	0.001
		2.4	5.6	58957	243	6929	84	0.117	0.001
		5.6	10.8	15894	126	2595	51	0.163	0.003

The correction procedure was checked by evaluating the lifetime of  $K_S^0$  and  $\Lambda$  from the corrected distribution of distances between the production and decay vertices. The proper decay length ( $c\tau$ ) distributions for  $K_S^0$  mesons and  $\Lambda$  hyperons are shown in Fig. 9.

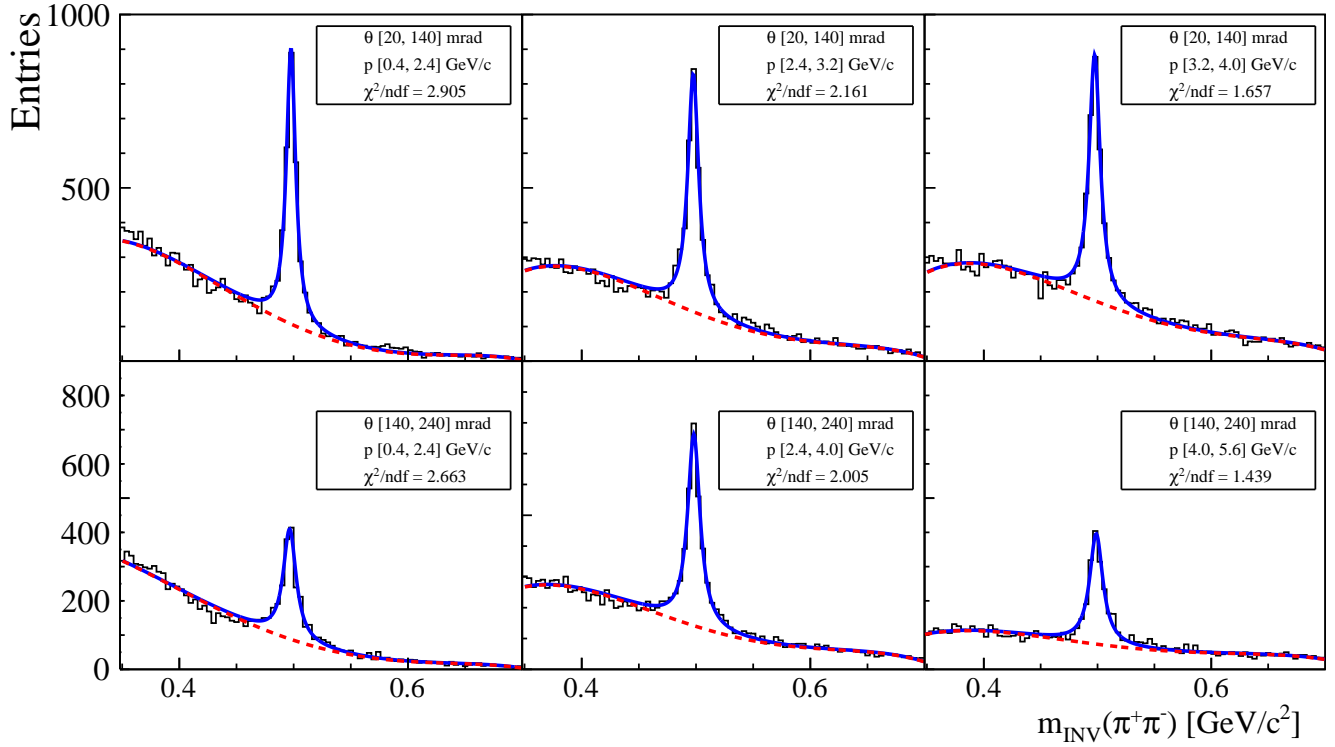


Figure 7: The invariant mass distributions for simulated  $K_S^0$  candidates in selected  $\{p, \theta\}$  bins.

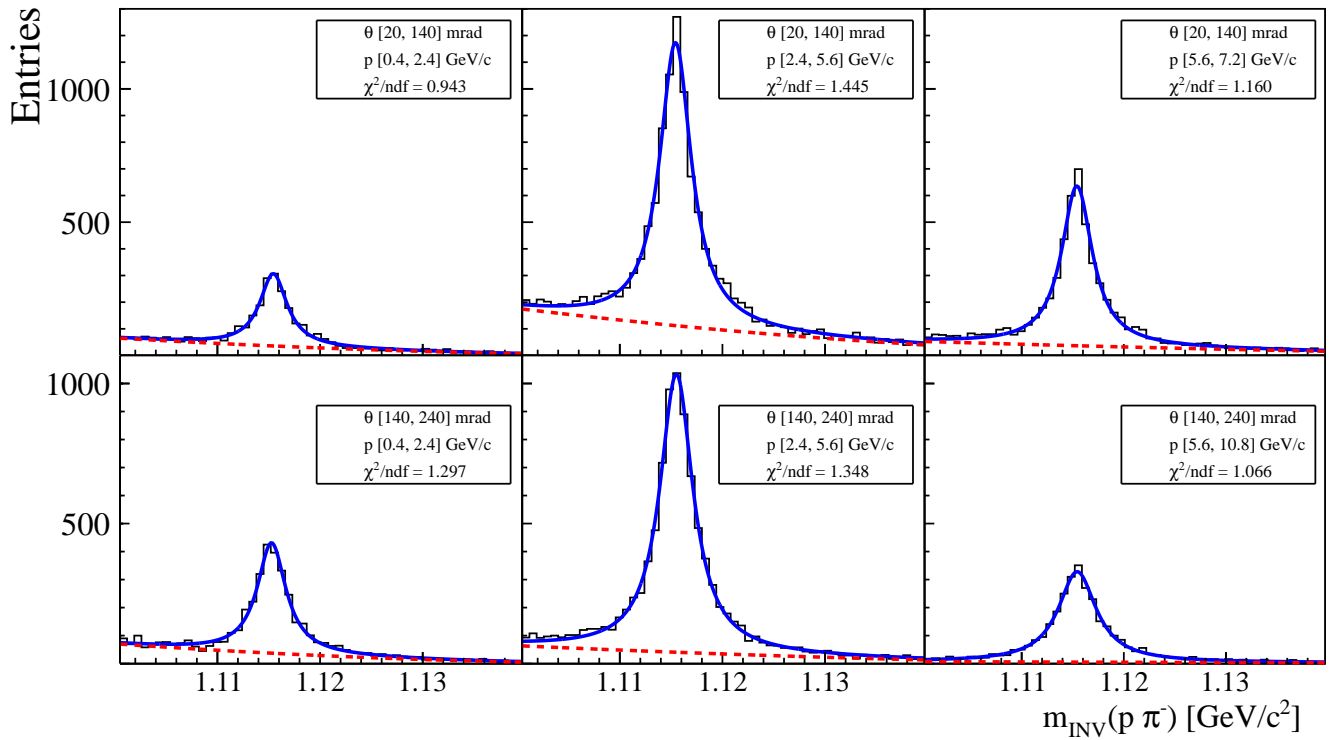


Figure 8: The invariant mass distributions for simulated  $\Lambda$  candidates in selected  $\{p, \theta\}$  bins.

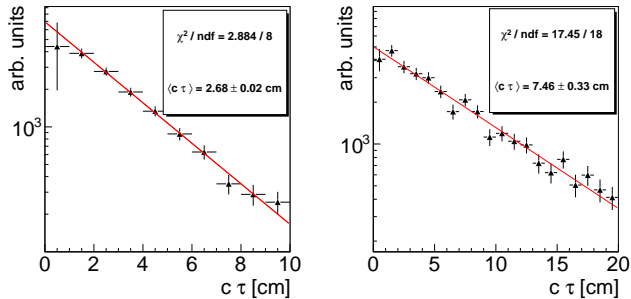


Figure 9: The proper decay length ( $c\tau$ ) distributions for  $K_S^0$  mesons (top) and  $\Lambda$  hyperons (bottom).

The obtained average proper decay lengths of  $2.68 \pm 0.02$  cm for  $K_S^0$  and  $7.46 \pm 0.33$  cm for  $\Lambda$  are consistent with the world averages.

The contribution of non-target interactions has small impact on the final results. The ratio B was found to be equal to  $2.198 \pm 0.027$ . After all cuts there were no  $V^0$  candidates found in the data recorded with target removed. Therefore, the subtraction procedure for out of target interactions changes only the number of events used for the normalization of spectra. The values of  $N^I$  and  $N^I\text{-BN}^R$  were 276481 and 276421, respectively.

#### D. Systematic errors

The main sources of the systematic uncertainty are as follows.

- (i) The uncertainty connected with the track cuts. The contribution of this source was studied by varying all standard track cuts (see Sec. III A). In particular the minimum distance between the primary vertex and the  $V^0$  decay point was varied from 3 cm to 6 cm. The invariant mass window was changed to  $[0.4, 0.65]$  GeV/ $c^2$  and to  $[1.09, 1.16]$  GeV/ $c^2$  for  $K_S^0$  and  $\Lambda$ , respectively. The accepted region for the  $\cos \epsilon$  was reduced to  $[-0.8, 0.6]$  for  $K_S^0$  and to  $[-0.7, 0.7]$  for  $\Lambda$ . The cuts in the Armenteros-Podolanski plots were varied by about 10%.
- (ii) The uncertainty connected with the background function used in the fitting procedure. Apart from the standard 4<sup>th</sup> order polynomial a set of different background functions was tried (3<sup>rd</sup> order polynomial, 6<sup>th</sup> order Chebyshev polynomial, Argus function).
- (iii) The uncertainty connected with the fitting procedure. Due to the low statistics of the data, fit results depend on the fit strategy and the limits set for the parameters. The most prominent effect was observed when the width of the signal function

was varied. The initial values of the position and the width of the signal were taken from the large statistic MC simulations and the variation within  $\pm 10 \cdot \Delta F_{MC}$  was used for the systematic error studies.

- (iv) The uncertainty connected with the inaccurate description of the reconstructed primary vertex distribution in the Monte Carlo.
- (v) The uncertainty connected with the inaccuracy of the geometrical acceptance obtained from Monte Carlo simulation, reconstruction efficiency, and different algorithms used for track merging.
- (vi) The uncertainty connected with the  $\{p, \theta\}$  bin size due to imperfect modeling of  $K_S^0$  and  $\Lambda$  spectra in the Monte Carlo. This effect was only studied in the  $K_S^0$  case by looking at the distributions in different Monte Carlo generators.

The systematic errors connected with uncertainties discussed in points (i) and (iv) were found to be almost momentum independent. The uncertainties discussed in point (v) depend strongly on the selected  $\{p, \theta\}$  bin. The systematic errors were estimated following the procedure presented in Refs. [5, 6].

The final systematic errors, calculated as the sum in quadrature of errors connected with the uncertainties discussed above, were found to be about 13.5-20.0% for  $K_S^0$  and  $\Lambda$  depending on the emission angle interval. The largest contributions always come from the uncertainty connected with the fitting approach (iii) and the uncertainty connected with the fit of the background (ii). Typical systematic errors connected with these sources were about 8-12% (iii) and about 7-8% (ii). The second most important contribution is related to the track cuts (i) and it is typically 4-5%. In addition important contribution comes from an inaccurate agreement between the data and Monte Carlo distributions of the fitted  $z$  coordinate of the primary vertex (iv). The systematic error connected with this effect is about 5%. The contributions connected with geometrical acceptance, reconstruction efficiency, and different reconstruction algorithms (v) are 3-4%, 2% and 2%, respectively. The systematic error connected with bin size (vi) was found to be about 6% in highly populated bins and about 12% in low statistic bins.

## IV. RESULTS

Differential inclusive cross sections were derived following the procedure described in Sec. III. They are tabulated in Tables IV and V as well as plotted in polar angle slices in Figs. 10 and 11 for  $K_S^0$  and  $\Lambda$ , respectively.

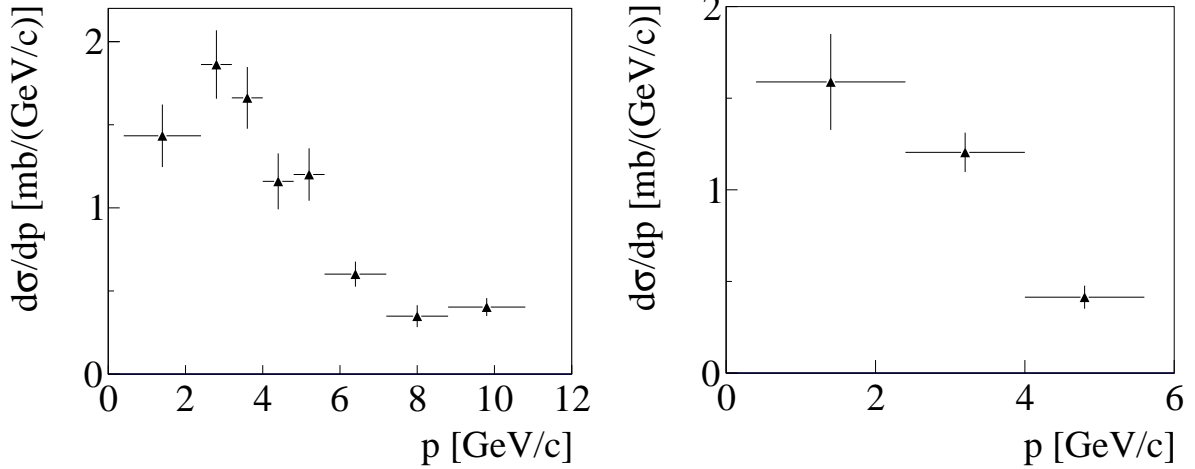


Figure 10:  $K_S^0$  production cross sections in two polar angle intervals: [20, 140] mrad (left) and [140, 240] mrad (right). Only statistical errors are shown. The normalization uncertainty is not included.

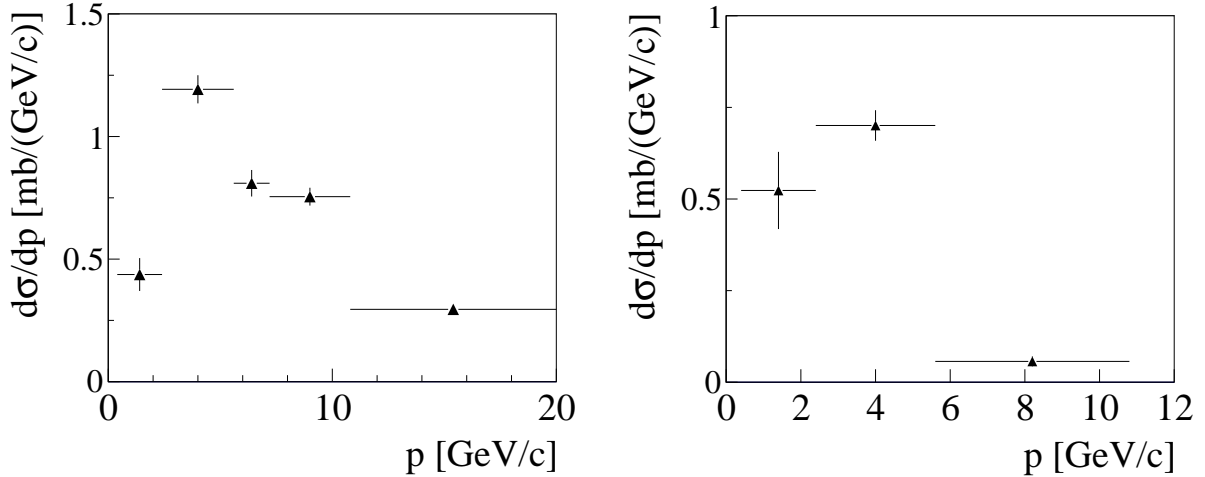


Figure 11:  $\Lambda$  production cross sections in two polar angle intervals: [20, 140] mrad (left), [140, 240] mrad (right). Only statistical errors are shown. The normalization uncertainty is not included.

The mean multiplicity in production processes and the inclusive cross section for  $K_S^0$  production were evaluated from the results obtained in momentum and polar angle intervals. Regions outside the geometrical acceptance were corrected according to the VENUS 4.12 model [10] which predicts 23.91% of simulated  $K_S^0$  to be outside of our  $\{p, \theta\}$  bins. In the UrQMD [12] model this number

is 20.27%.

The spread of model predictions was used to estimate the systematic error of the extrapolation to full phase space.

The final results with systematic errors are as follows.

The  $K_S^0$  mean multiplicity in production processes is  $\langle n_{K_S^0} \rangle = 0.127 \pm 0.005$  (stat)  $\pm 0.022$  (sys) .

Table IV: The NA61/SHINE results for the differential  $K_S^0$  production cross section in the laboratory system for p+C interactions at 31 GeV/c.

$\theta_{\text{low}}$	$\theta_{\text{up}}$	$p_{\text{low}}$	$p_{\text{up}}$	$d\sigma_{K_S^0} / dp$	$\Delta_{\text{stat}}$	$\Delta_{\text{stat}}$	$\Delta_{\text{sys}}$
(mrad)	(mrad)	(GeV/c)	(GeV/c)	(mb/GeV/c)	[%]	[%]	[%]
0	20	0.4	7.2	0.061	0.010	16.8	18.4
20	140	0.4	2.4	1.434	0.188	13.1	17.8
		2.4	3.2	1.862	0.206	11.0	15.5
		3.2	4.0	1.662	0.186	11.2	14.4
		4.0	4.8	1.159	0.168	14.5	14.4
		4.8	5.6	1.200	0.158	13.1	14.4
		5.6	7.2	0.601	0.075	12.5	14.4
		7.2	8.8	0.348	0.066	18.9	14.4
		8.8	10.8	0.403	0.054	13.4	16.3
140	240	0.4	2.4	1.589	0.26	16.5	19.5
		2.4	4.0	1.204	0.139	8.9	14.4
		4.0	5.6	0.414	0.063	15.2	14.4
		5.6	10.8	0.073	0.011	14.6	16.9
		240	420	0.4	5.6	0.938	0.182

Table V: The NA61/SHINE results for differential  $\Lambda$  production cross section in the laboratory system for p+C interactions at 31 GeV/c.

$\theta_{\text{low}}$	$\theta_{\text{up}}$	$p_{\text{low}}$	$p_{\text{up}}$	$d\sigma_{\Lambda} / dp$	$\Delta_{\text{stat}}$	$\Delta_{\text{stat}}$	$\Delta_{\text{sys}}$
(mrad)	(mrad)	(GeV/c)	(GeV/c)	(mb/GeV/c)	[%]	[%]	[%]
20	140	0.4	2.4	0.437	0.067	15.3	16.8
		2.4	5.6	1.193	0.057	4.8	16.1
		5.6	7.2	0.809	0.054	6.7	15.9
		7.2	10.8	0.755	0.036	4.8	16.6
		10.8	20.0	0.295	0.016	5.3	16.8
140	240	0.4	2.4	0.523	0.105	20.1	16.6
		2.4	5.6	0.701	0.042	5.9	15.9
		5.6	10.8	0.057	0.013	23.7	16.8

The inclusive cross section for  $K_S^0$  production is  $\sigma_{K_S^0} = 29.0 \pm 1.6$  (stat)  $\pm 5.0$  (sys) [mb].

Due to different phase-space distributions of  $\Lambda$  and  $K_S^0$  a model-dependent correction for a unmeasured yield of  $\Lambda$  hyperons is about two times larger than the one for  $K_S^0$  mesons. Therefore a reliable extrapolation of the  $\Lambda$  hyperon yield to the full phase was not possible.

The  $K_S^0$  mean multiplicity in production processes from p+C interactions was compared with a compilation [13] of total integrated  $K_S^0$  yields from p+p interaction experiments. For this purpose the NA61/SHINE result was scaled according to the Wounded Nucleon Model (WNM) by a multiplicative scaling factor  $2/(1+\langle n_W \rangle)$  and according to the Independent Collisions Model (ICM) by a multiplicative scaling factor  $1/\langle n_W \rangle$ , where  $\langle n_W \rangle$  is the average number of wounded nucleons inside

the carbon nucleus. The value of  $\langle n_W \rangle$  was found to be  $1.5240 \pm 0.0011$  using the GLauber Initial-State Simulation AND mOre (GLISSANDO) model calculation [14]. The comparison of our result with the compilation of existing p+p results is shown in Fig. 12. Better agreement is observed between the scaled NA61/SHINE result and the measurement for p+p interactions when the ICM scaling is used. The larger value of the kaon multiplicity ( $0.127 \pm 0.005$ ) as compared to the WNM model ( $0.063 \times 1.26 = 0.0793$ ) can be regarded as an indication of enhanced strange particle production in p+C collisions at 31 GeV/c. However, a definitive conclusion is not possible due to the systematic uncertainties of our results.

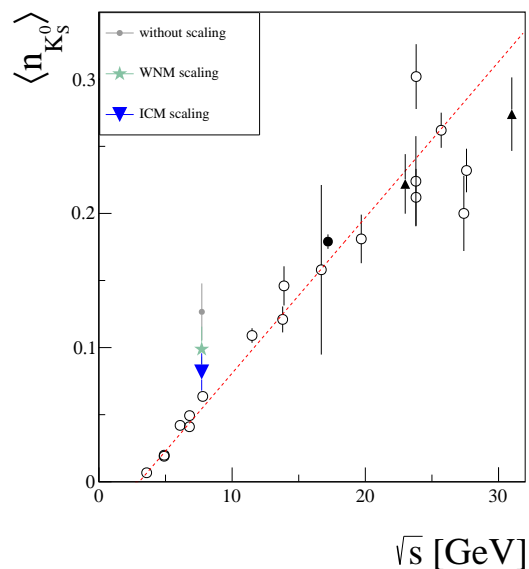


Figure 12: Mean multiplicity of  $K_S^0$  mesons as a function of  $\sqrt{s}$ . Open black points: p+p results from the compilation [13]. Full circle: the NA49 result on  $((K^+ + K^-)/2)$  [13]. Triangles: the ISR measurements of  $((K^+ + K^-)/2)$  and the UA5 results [13]. Grey circle: the result from this paper for p+C interactions. Green full star: the result from this paper after scaling according to the WNM model. Blue triangle: the result from this paper after scaling according to the ICM model. The dashed line is shown to guide the eye.

## V. COMPARISON WITH MODEL PREDICTIONS

The  $K_S^0$  results in momentum and polar angle variables normalized to mean particle multiplicity in production processes are shown in Fig. 13 with predictions from the hadron production models VENUS and UrQMD superimposed.

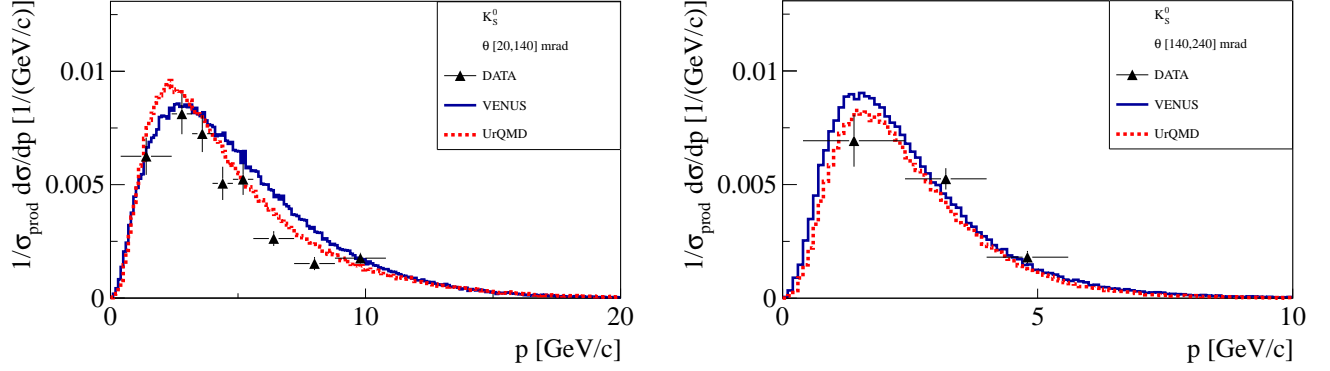


Figure 13: Mean multiplicity of  $K_S^0$  mesons in production processes in polar angle intervals: [20, 140] mrad (left), [140, 240] mrad (right). Two hadron production model predictions are superimposed. Only statistical errors are shown.

The  $K_S^0/\pi^-$  ratio is plotted versus momentum for selected polar angle intervals in Fig. 14. The  $\pi^-$  spectra were taken from Ref. [5]. The ratio of  $K_S^0/\pi^-$  is expected to be close to the ratio of the  $\bar{s}$  to  $\bar{u}$  quark production probabilities and it is therefore sensitive to the strangeness suppression factor,  $\lambda_s$ . Furthermore, the ratio  $K_S^0/\pi^-$  is used in the calculation of the feed-down corrections when extracting primary pion multiplicities from the data. In Ref. [5] VENUS model predictions, not yet confronted with the NA61/SHINE measurements, were used and therefore large systematic errors were assigned. It is seen from Fig. 14 that the agreement between data and the model is rather satisfactory for the emission angle interval 20-140 mrad whereas the disagreement is large at larger angles. The measured average multiplicity of  $K_S^0$  differs by about 20% from the one predicted by VENUS and used in the NA61/SHINE correction procedure. The  $K_S^0/K^+$  ratio in the selected polar angle intervals is shown in Fig. 15. The  $K^+$  spectra were measured in the same experiment [6] therefore some of the systematic errors canceled out. The  $d/u$  quark ratio in  $p+C$  interactions is 5:7. The smaller yield of  $K_S^0$  compared to that of  $K^+$  is thus expected because it is more probable to find a  $u$  current quark to form a positively charged kaon ( $u\bar{s}$ ) than a  $d$  quark to form a  $K^0$  ( $d\bar{s}$ ). The  $\bar{K}$  ( $\bar{d}s$ ) requires the production of two sea quarks and thus it is less frequent.

The  $\Lambda$  results in momentum and polar angle variables normalized to mean particle multiplicity in production processes are shown in Fig. 16 with the predictions from the hadron production models superimposed. None of the models provides a satisfactory description of our measurements.

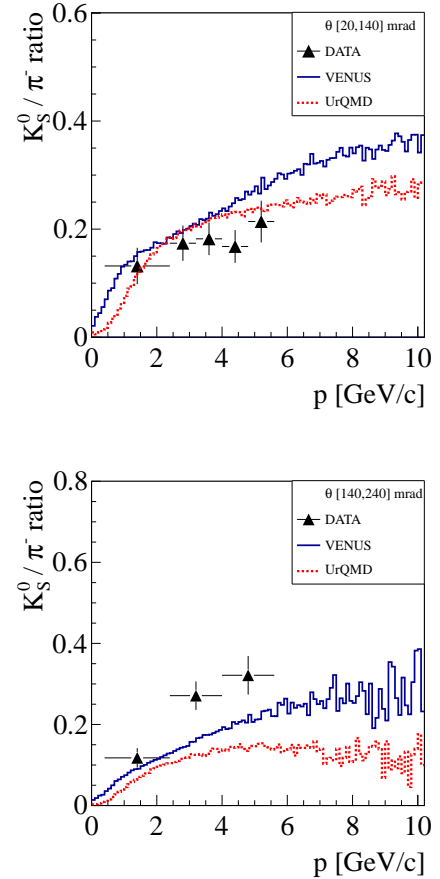


Figure 14:  $K_S^0/\pi^-$  ratios versus momentum in two polar angle intervals: [20, 140] mrad (top), [140, 240] mrad (bottom). The vertical error bars on the data points show the total (stat. and syst.) uncertainty. Predictions of two hadron production models are superimposed.

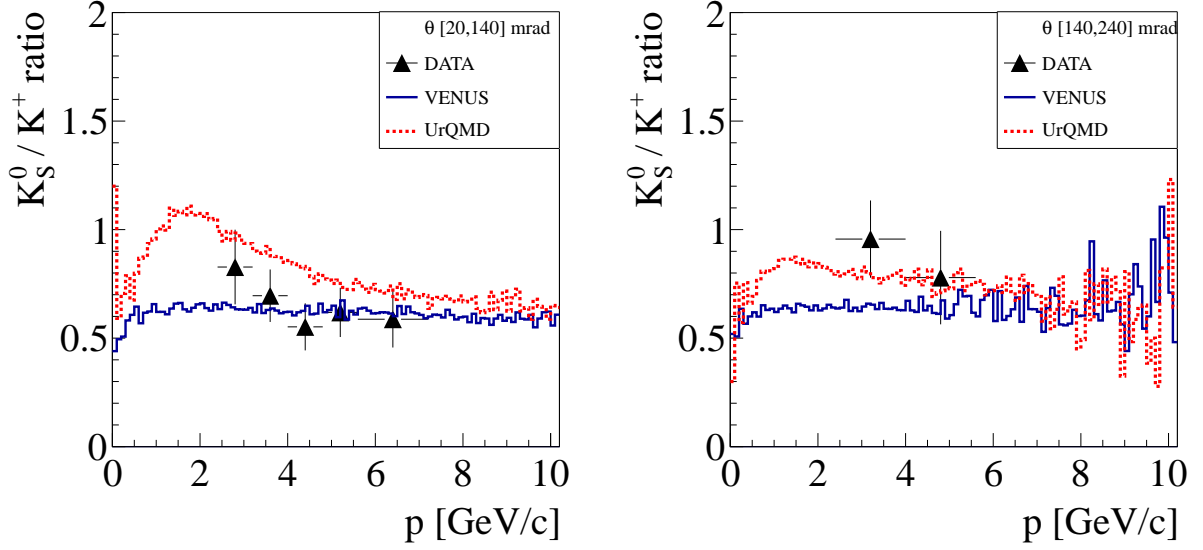


Figure 15:  $K_S^0/K^+$  ratios in two polar angle intervals in two polar angle bins [20, 140] mrad (top) and [140, 240] mrad (bottom). The vertical error bars on the data points show the total (stat. and syst.) uncertainty. Predictions of hadron production models are superimposed.

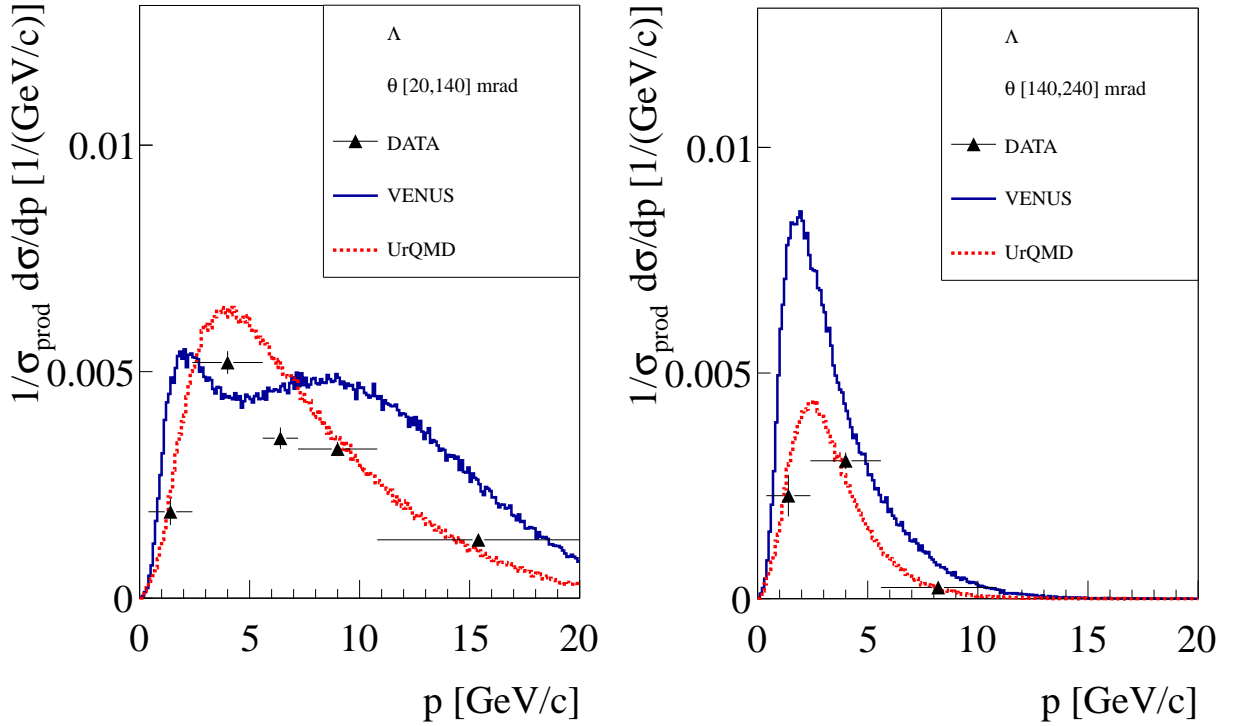


Figure 16: Mean multiplicity of  $\Lambda$  hyperons in production processes in polar angle intervals: [20, 140] mrad (top), [140, 240] mrad (bottom). Hadron production model predictions are superimposed. Only statistical errors are shown.

## VI. SUMMARY

We present the first measurement of the total cross section for  $K_S^0$  production in p+C interactions at 31 GeV/c in the experimentally sparsely covered region of a few tens of GeV/c beam momentum. The increase of the mean  $K_S^0$  multiplicity with respect to p+p collisions can be explained within errors by a factor equal to the average number of primary proton interactions in the carbon nucleus. Differential cross sections for  $K_S^0$  and  $\Lambda$  production were obtained in bins of laboratory momentum and emission angle and are compared with predictions of several hadron production models. Significant discrepancies between our experimental results and predictions of the VENUS 4.12 and UrQMD models are observed. These new measurements will help to further refine the prediction of the neutrino beam flux in the T2K experiment.

## VII. ACKNOWLEDGMENTS

This work was supported by the Hungarian Scientific Research Fund (grants OTKA 68506 and 71989), the Polish Ministry of Science and Higher Education

(grants 667/N-CERN/2010/0, NN 202 48 4339 and NN 202 23 1837), the National Science Centre of Poland, grant UMO-2012/04/M/ST2/00816, the Foundation for Polish Science - MPD program, co-financed by the European Union within the European Regional Development Fund, the Federal Agency of Education of the Ministry of Education and Science of the Russian Federation (grant RNP 2.2.2.2.1547), the Russian Academy of Science and the Russian Foundation for Basic Research (grants 08-02-00018, 09-02-00664 12-02-91503-CERN), the Ministry of Education, Culture, Sports, Science and Technology, Japan, Grant-in-Aid for Scientific Research (grants 18071005, 19034011, 19740162, 20740160 and 20039012), the German Research Foundation (grants GA 1480/2-1 and GA 1480/2-2), the Bulgarian National Scientific Foundation (grant DDVU 02/19/ 2010), the Ministry of Education and Science of the Republic of Serbia (grant OI171002), the Swiss National funds Foundation (grant 200020-117913/1) and ETH Research Grant TH-01 07-3.

Finally, it is a pleasure to thank the European Organization for Nuclear Research for a strong support and hospitality and, in particular, the operating crews of the CERN SPS accelerator and beam lines who made the measurements possible.

- 
- [1] P. Zh. Aslanyan *et al.*, Phys. Part. Nucl. Lett. **4**, 60 (2007).
  - [2] K. Jaeger *et al.*, Phys. Rev. **D11**, 1756 (1975).
  - [3] M. Yu. Bogolyubsky *et al.*, Sov. J. Nucl. Phys.**50**, 424 (1989).
  - [4] V. V. Ammosov *et al.*, Nucl. Phys. **B115**, 269 (1976).
  - [5] N. Abgrall *et al.* [NA61/SHINE Collaboration], Phys. Rev. **C84**, 034604 (2011); arXiv: 1102.0983.
  - [6] N. Abgrall *et al.* [NA61/SHINE Collaboration], Phys. Rev. **C85**, 035210 (2012).
  - [7] I. Abt *et al.* [HERA-B Collaboration], Eur. Phys. J. C **61**, 207 (2009) [Erratum-ibid. C **64**, 167 (2009)] [arXiv:0812.0471 [hep-ex]].
  - [8] N. Antoniou *et al.* [NA49-future Collaboration], CERN-SPSC-2006-034, (2006).
  - [9] S. Afanasev *et al.* [NA49 Collaboration], Nucl. Instrum. Meth. A **430**, 210 (1999).
  - [10] K. Werner, Nucl. Phys. **A525**, 501c (1991); Phys. Rep. **232**, 87 (1993).
  - [11] C. Strabel, Ph.D. Thesis, ETH Zurich (2011), <https://edms.cern.ch/document/1136130/1>.
  - [12] S. Bass *et al.*, Prog. Part. Nucl. Phys. **41**, 255 (1998); V. Uzhinsky, arXiv:1107.0374.
  - [13] T. Anticic *et al.* [NA49 Collaboration], Eur. Phys. J. **iC68**, 1 (2010).
  - [14] W. Broniowski *et al.*, Comput. Phys. Commun. **180**, 69 (2009).
  - [15] T. Czopowicz, thesis, Warsaw University of Technology (2010), <https://edms.cern.ch/document/1138108/1>.
  - [16] K. Aamodt *et al.* [ALICE Collaboration], Eur. Phys. J. **C71**, 1594 (2011).
  - [17] K. Werner, Nuclear Physics B Proc. Suppl., **175-176**, 81 (2008).